JACS
JOURNAL OF THE AMERICAN CHEMICAL SOCIETY
Communication
pubs.acs.org/JACS

Stabilization of High-Performance Oxygen Reduction Reaction Pt Electrocatalyst Supported on Reduced Graphene Oxide/Carbon Black Composite

Yujing Li,[†,§] Yongjia Li,[†] Enbo Zhu,[†] Tait McLouth,[†] Chin-Yi Chiu,[†] Xiaoqing Huang,[†] and Yu Huang*[,†,‡]

[†]Department of Materials Science and Engineering and [‡]California NanoSystems Institute, University of California, Los Angeles, California 90095, United States

Supporting Information

ABSTRACT: Oxygen reduction reaction (ORR) catalyst supported by hybrid composite materials is prepared by well-mixing carbon black (CB) with Pt-loaded reduced graphene oxide (RGO). With the insertion of CB particles between RGO sheets, stacking of RGO can be effectively prevented, promoting diffusion of oxygen molecules through the RGO sheets and enhancing the ORR electrocatalytic activity. The accelerated durability test (ADT) demonstrates that the hybrid supporting material can dramatically enhance the durability of the catalyst and retain the electrochemical surface area (ECSA) of Pt: the final ECSA of the Pt nanocrystal on the hybrid support after 20 000 ADT cycles is retained at >95%, much higher than the commercially available catalyst. We suggest that the unique 2D profile of the RGO functions as a barrier, preventing leaching of Pt into the electrolyte, and the CB in the vicinity acts as active sites to recapture/renucleate the dissolved Pt species. We furthermore demonstrate that the working mechanism can be applied to the commercial Pt/C product to greatly enhance its durability.

Precious metal group (PMG) nanocrystals (NCs) have so far shown the greatest potential as cathode electrocatalysts in proton exchange membrane fuel cells.[1] Synthesis of highly active PMG nanocatalysts has intrigued chemists for the past decade.[2−5] To make the most use of the precious metal and reduce the cost of fuel cells, PMG NCs are usually loaded on high surface area supporting materials.[6] Carbon-based materials have been widely used as supporting material for PMG catalysts.[7−12] The activity and durability of carbon-supported PMG NCs in the oxygen reduction reaction (ORR) occurring at the fuel cell cathode are of great concern to both industry and academia.[6] So far, high surface area carbon black (CB), carbon nanotubes, highly oriented pyrolytic graphite, etc., have been systematically studied as ORR catalyst supports.[13−16] Recently, graphene (or reduced graphene oxide, RGO) has attracted attention as a unique 2D material with good conductivity, high surface area, and high mechanical strength—requirements of a good electrocatalyst support.[17] Thus, intensive effort has focused on using RGO as a catalyst support for the ORR, and some exciting results have been reported.[18−27]

However, due to the nature of the 2D material, RGO sheets tend to stack together through $\pi-\pi$ interaction when they are dried, even when they are loaded with NCs.[22] The stacking blocks a substantial amount of catalytic sites on NCs and sets a higher resistance for the diffusion of reactant molecules, which retards the catalytic reaction. Various reported works on RGO-supported ORR catalysts show retarded oxygen reduction rates at a certain potential range and slowed oxygen diffusion.[18,28,29] In addition, RGO sheets obtained by wet chemical synthesis usually contain more defects, which reduces the electron-transfer rate in the graphene sheet and across the NC-RGO interface as well.[30] So far, little effort has been made to address this issue and to prevent the stacking of RGO sheets as the support.[31,32]

We report an approach to design highly active and durable ORR catalyst by loading Pt NCs on a primary support RGO, which then is composited with a secondary high surface area CB support. By inserting CB particles between the Pt/RGO sheets, the composite structure not only enhances the catalytic activity but also dramatically improves the durability of the catalyst.

Pt NCs were synthesized in an aqueous solution at 85 °C (see Supporting Information for experimental details.) A TEM image of the as-synthesized water-soluble Pt NCs is shown in Figure S1; >80% of the NCs show cuboctahedral morphology with uniform size. The average size is 5 nm with <5% deviation. The high-resolution image in Figure S1b shows that the as-synthesized Pt NCs are single-crystalline.

The weight concentration of the Pt NCs in solution was measured by inductively coupled plasma optical emission spectrometry (ICP-OES) to estimate the amount of carbon materials needed to achieve the expected Pt/C ratio. Pt NCs loaded on different types of supports are shown in Figure 1. On RGO, the Pt loading ratio is 33 wt% (referred to total mass). TEM shows that Pt NCs were loaded uniformly on RGO without obviously localized aggregation. RGO was obtained by hydrazine reduction of graphene oxide synthesized by modified Hummers method.[33,34] Pt/RGO/CB composite was prepared by mixing Pt/RGO with CB in IPA and stirring overnight. According to Figure 1c, the typical view under TEM, all Pt-loaded RGO sheets form composites with CB particles. We note that no bare Pt/RGO sheets or bare CB without NCs were observed by TEM, indicating well-mixed nature of the composite. Besides, most Pt

Received: April 1, 2012
Published: July 11, 2012

 © 2012 American Chemical Society dx.doi.org/10.1021/ja3031449 | J. Am. Chem. Soc. 2012, 134, 12326−12329

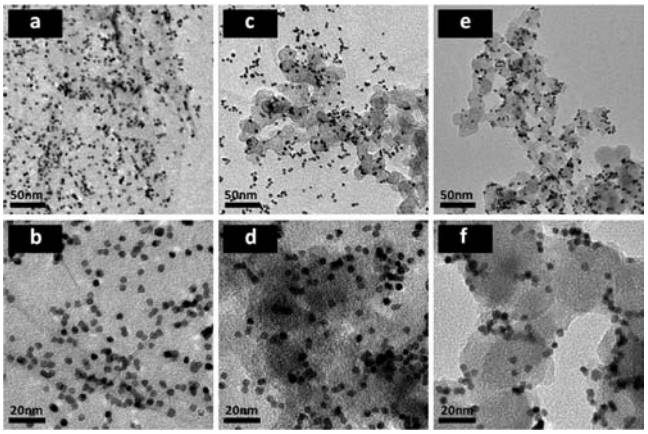

Figure 1. TEM images of (a,b) Pt NCs loaded on RGO, (c,d) Pt/RGO mixed with CB (Pt/RGO/CB-1), and (e,f) Pt NCs loaded only on CB.

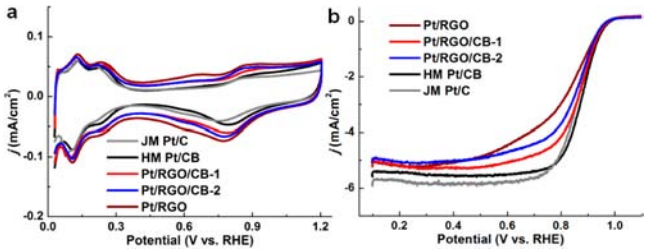

Figure 2. (a) CV and (b) polarization curves for HM Pt/CB, Pt/RGO, JM Pt/C, and Pt/RGO/CB-1 and -2.

NCs were still attached on the RGO, indicating good contact between Pt NCs and RGO. As a comparison, TEM images of Pt NCs directly loaded on CB are shown in Figure 1e,f. There is an obvious difference in how Pt NCs are located on Pt/CB versus on the Pt/RGO/CB. Two types of Pt/RGO/CB catalysts were prepared with RGO/CB (note: not the ratio between Pt/RGO and CB) mass ratios of 1:1 (termed Pt/RGO/CB-1) and 2:1 (Pt/RGO/CB-2). The loading ratio of Pt on Pt/RGO/CB-1 (Figure 1c,d) is 22 wt%, Pt on Pt/RGO/CB-2 is 26 wt%, and Pt on homemade (HM) Pt/CB is 21 wt%, determined by thermal gravimetric analysis.

Electrochemical measurement was carried out to observe the effect of CB insertion on ORR. Loading of Pt on a glassy carbon electrode (GCE) was controlled at 13.8 $\mu g/cm^2$ for all catalyst samples with HM Pt NCs. Commercial Pt/C catalyst (20 wt% Pt on Vulcan XC72R carbon) obtained from Johnson Matthey (termed JM Pt/C) was used as a baseline catalyst for comparison. Due to the difficulty of making a uniform catalyst film with JM Pt/C at the same loading amount, loading of JM Pt/C was controlled at 20.4 $\mu g/cm^2$. After the electrode was fully activated with cyclic voltammetry (CV) scans between 0 and 1.0 V (vs reversible hydrogen electrode), the stable CV curves were recorded (Figure 2a). All CV curves were normalized by corresponding electrochemical surface areas (ECSAs) calculated by integrating hydrogen adsorption charges.[35] The specific ECSAs of these catalysts were measured to be 60.1, 57.0, 56.4, and 50.0 m^2/g for HM Pt/CB, Pt/RGO, and Pt/RGO/CB-1 and -2, compared with 58.9 m^2/g for JM Pt/C.

Polarization curves in O_2-saturated $HClO_4$ electrolyte were recorded on a rotating disk electrode at a rotating rate of 1600 rpm, normalized by the area of the GCE (0.196 cm^2) (Figure 2b). Compared with HM Pt/C catalyst, Pt/RGO shows a much lower current density at 0.9 V, indicating that the kinetic current is

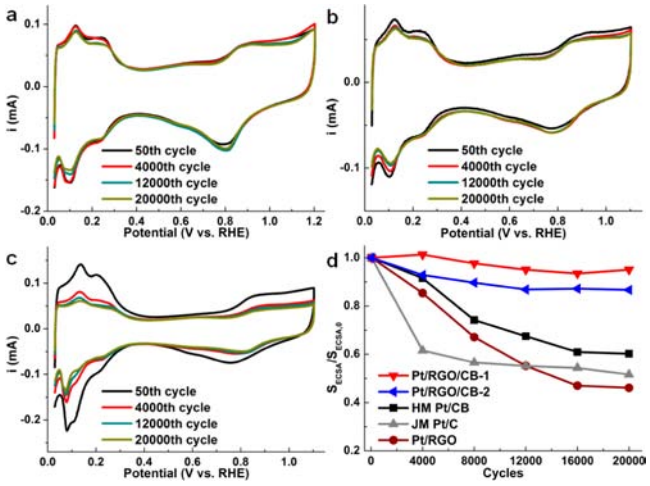

Figure 3. CV curves of 50, 4000, 12 000, and 20 000 cycles for (a,b) Pt/RGO/CB-1 and -2 and (c) JM Pt/C. (d) Comparison of ECSA loss for different materials. $S_{ECSA,0}$ is initial ECSA of corresponding catalyst.

lower when Pt NCs are loaded on RGO. In addition, the diffusion-limiting potential region (where current is stabilized as a plateau) is shorter for the Pt/RGO catalyst, meaning that its kinetic current drops faster with elevating potential. However, for the HM Pt/CB catalyst, the current at mixed kinetic-diffusion control region (between 0.80 and 0.95 V) is higher than for a commercial JM Pt/C catalyst. All the above information indicates that the RGO-supported Pt NCs show lower ORR activity than Pt NCs on CB and that pure RGO inhibits the oxygen reduction rate. This is partly because when Pt/RGO catalyst is dried, RGO sheets tend to form a closely packed film, inhibiting diffusion of O_2 through the film to approach the Pt surface, thus lowering the reduction rate on Pt NCs.[36] SEM images in Figure S2c,d show stacking of the Pt-loaded RGO. Interestingly, when CB is mixed well with Pt-loaded RGO sheets as a secondary support, currents can be dramatically promoted between 0.6 and 0.9 V, indicating that the ORR activity can be recovered. This is because the inserted CB particles enlarge the gaps between RGO sheets, providing enough space for fast oxygen diffusion through the film and enhancing the oxygen supply in the film, accelerating the reduction rate. The structure of the well-mixed composite is shown in Figure S3, with the Pt-loaded RGO sheet (highlighted with yellow circles) sandwiched by CB particles (highlighted with black circles). Comparing the polarization curves of Pt/RGO/CB-1 and -2 samples, it can be seen that when more CB is added, more space is created and ORR activity can be further enhanced, confirming the proposed inhibition mechanism of RGO and the recovery mechanism by adding CB.

ADT was carried out to test the durability of the catalysts. Potential was cycled between 0.6 and 1.1 V in 0.1 M $HClO_4$, which was exposed to the atmosphere. CV curves between 0 and 1.1 V were recorded every 4000 cycles to compare the ECSAs during potential cycling. Figure 3a,b shows the evolutions of CV curves for Pt/RGO/CB-1 and -2, with the change of JM Pt/C shown in Figure 3c as a comparison. Similar curves for HM Pt/CB and Pt/RGO are shown in Figure S4. It is observed that the ECSA of JM Pt/C drops to almost 60% of its initial surface area after the first 4000 ADT cycles, but the loss slows down, and the final ECSA after 20 000 cycles stabilizes at ~51% of the initial value, consistent with previously reported results (Figure 3d).[37] For the HM Pt/CB catalyst, the ECSA slowly drops to 60%, slightly better than the commercial JM Pt/C catalyst. The Pt/

dx.doi.org/10.1021/ja3031449 | J. Am. Chem. Soc. 2012, 134, 12326–12329

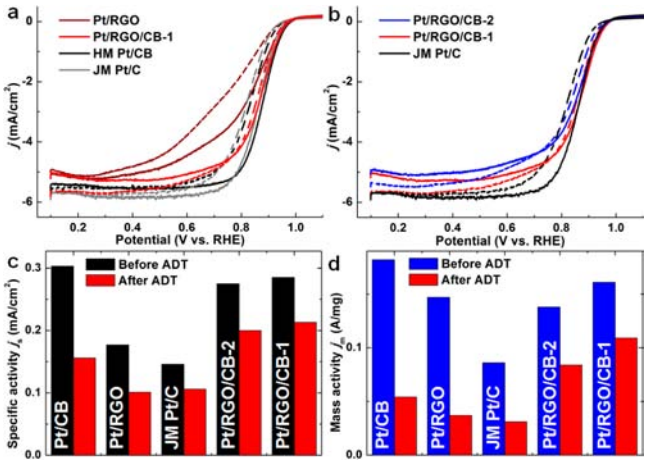

Figure 4. Polarization curves of (a) Pt/CB, Pt/RGO, JM Pt/C, and Pt/RGO/CB-1, and (b) Pt/RGO/CB-1 and -2 with comparison of JM Pt/C, before (solid curves) and after (dashed curves) the ADT. (c,d) Specific and mass activities at 0.9 V for different materials.

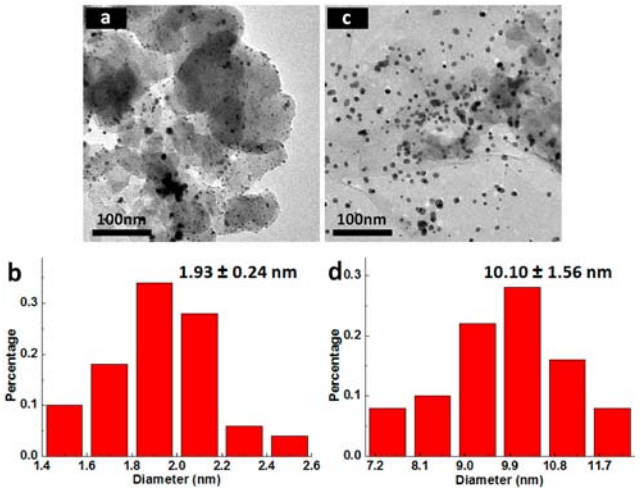

Figure 5. (a,c) TEM images of Pt particles supported on CB and on RGO, respectively, from collected Pt/RGO/CB-1 after ADT, captured in different regions from the same TEM sample. (b,d) Statistical analyses of Pt sizes supported on CB and on RGO, respectively, as shown in (a,c).

RGO retains only 46% of its initial ECSA. However, the Pt/RGO/CB-2 sample shows improvement on ECSA loss, with 87% of the initial ECSA remaining. With higher additions of CB, the Pt/RGO/CB-1 sample retains >95% of its initial ECSA.

ORR activities after 20 000 cycles of ADT were also measured for all samples in O_2-saturated $HClO_4$ electrolyte. Figure 4a shows the polarization curves for HM Pt/CB, Pt/RGO, Pt/RGO/CB-1, and JM Pt/C catalysts; polarization before and after the ADT is shown in solid and dashed curves, respectively. In the mixed kinetic-diffusion control region, it is obvious that the polarization curves of the Pt NCs on CB or RGO only show a more obvious current drop after the ADT, while there is almost no change for the Pt/RGO/CB-1 sample which is supported on the RGO/CB composite. To illustrate the effect of CB amount added into the Pt/RGO catalyst, Figure 4b compares Pt/RGO/CB-1 and -2 with JM Pt/C, indicating the better performance of Pt/RGO/CB-1 and -2 over the commercial JM Pt/C catalyst. Activities were calculated as a quantitative comparison to illustrate the superior performance of Pt/RGO/CB catalysts. Mass-transport-corrected kinetic current at 0.9 V was calculated according to the Levich–Koutecký equation: $1/i = 1/i_k + 1/i_d$, where i_k is the kinetic current and i_d is the diffusion-limiting current.[38] As shown in Figure 4c, after the ADT, the specific activities of Pt/RGO/CB-1 and -2 samples at 0.9 V are 0.212 and 0.200 mA/cm^2, respectively, almost twice that of the commercial JM Pt/C catalyst (~0.106 mA/cm^2) and higher than those supported only on CB or RGO. In terms of mass activity, the Pt/RGO/CB-1 sample remains at 0.109 A/mg after ADT, slightly higher than the activity of Pt/RGO/CB-2 sample and triple the final mass activity of the commercial JM Pt/C after ADT (0.031 A/mg). Both Pt/RGO/CB samples show significantly smaller change in activities than the commercial catalyst, indicating the obvious enhancement of the catalyst durability when CB is inserted into Pt/RGO.

To reveal the mechanism of the durability enhancement observed, catalysts were collected by sonicating the GCE in IPA after the ADT, and their structures were observed by TEM. TEM images of as-prepared HM Pt/CB and Pt/RGO (Figure S5) show the statistical analyses of the Pt NC sizes after the ADT test. In general the Pt NCs grow obviously in size through Ostwald ripening. The average sizes are ~9.75 and ~10.92 nm for Pt/CB and Pt/RGO, compared to ~5 nm before the ADT, and both with much wider size distributions. The commercial JM Pt/C catalysts grow in size from ~3 to ~12 nm after the ADT, as shown in Figure S6. This is consistent with the observed obvious decrease in ECSA for these catalysts. However, in the Pt/RGO/CB samples, after the ADT we found a significant portion of Pt NCs attached on CB, while all NCs were on RGO before the ADT. Interestingly, the size distributions of Pt NCs on CB and RGO are distinctively different. Figure 5a,c shows typical Pt NCs supported on CB and RGO, respectively, from Pt/RGO/CB-1 after ADT. The size of NCs attached on CB (~1.93 nm) is obviously smaller than that of the NCs on RGO sheets (~10.10 nm). It is interesting that the NCs attached on CB are much smaller than the initial Pt NCs loaded on RGO sheets (~5 nm). We suggest that, while the Pt NCs on RGO sheets experience Ostwald ripening, as do those on the regular samples, the Pt species or clusters dissolved during the ripening process can be recaptured or can renucleate on the CB in the hybrid support structure. It has been reported that the migration of Pt atoms or clusters on a carbon surface depends strongly on surface heterogeneity, which means that defects or kinks on the surface can serve as heterogeneous nucleation sites.[39,40] Compared with a smooth graphitized surface, CB is richer in kinks and traps, which provides more nucleation sites for migrating Pt species (atoms or clusters) and re-collects more Pt species which would otherwise combine into larger particles or dissolve into the electrolyte. So CB is potentially more capable of capturing migrating Pt species. This is consistent with our findings that the loss of Pt ECSA is lower on HM Pt/CB than on Pt/RGO (Figure 3d). In the Pt/RGO/CB, the CB can capture and provide nucleation sites for the migrating Pt species generated from dissolution of Pt NCs (induced by Ostwald ripening) on RGO, while the RGO sheets, with their 2D nature, can possibly act as a "mesh bag" to prevent the Pt species from leaking into the electrolyte, providing more opportunity to be captured or to renucleate on the CB component. This synergetic process creates many ultrasmall Pt NCs on the CB surface, which in turn counteracts the decreased Pt surface area induced by Pt ripening and dissolution. Hence we observed a sharp decrease in the total loss of ECSA for Pt/RGO/CB samples.

With the proposed mechanism, the high durability of the Pt/RGO/CB composite catalysts can be readily understood. The

dx.doi.org/10.1021/ja3031449 | J. Am. Chem. Soc. 2012, 134, 12326–12329

mechanism is further confirmed by control experiments with two additional types of catalysts prepared by mixing JM Pt/C catalyst with (1) RGO and (2) CB (see Supporting Information for details). The final ECSA of JM Pt/C/RGO after 20 000 cycles of ADT is >80% (Figure S7) of the initial ECSA, much higher than for the JM catalyst (51%) and JM Pt/C/CB (47%). It confirms that the presence of RGO is important in enhancing the durability and that this hybrid support structure can be broadly applicable to commercial catalytic products. Another catalyst structure, prepared by randomly mixing Pt/RGO and CB without the sonication and stirring process (Pt/RGO/CB-M, see Figure S8), was used to confirm the effect of the homogenous composite structure between Pt/RGO and CB. Figure S9 shows that the final ECSA of Pt/RGO/CB-M decreased to ~60% of the initial value, much worse than that of Pt/RGO/CB-1 (95%), indicating that a well-mixed RGO/CB composite structure is critical to achieving greatly enhanced durability. The above comparisons are consistent with the proposed mechanism.

In summary, we have demonstrated that the composite catalytic structure Pt/RGO/CB shows greatly enhanced ORR activity compared to the simple Pt/RGO structure in 0.1 M $HClO_4$. Importantly, ADT shows that the Pt/RGO/CB loses only 5% of its ECSA after up to 20 000 cycles of testing, while the commercial JM Pt/C catalyst loses almost 50% of its ECSA after the same number of cycles. In addition, the ORR mass activity of the Pt/RGO/CB catalyst after the ADT is twice that of the commercial JM Pt/C catalyst. TEM observations combined with electrochemical measurements suggest that, in the hybrid structure, the flexible 2D profile of RGO may function as a "mesh" that prevents leaching of dissolved Pt species into the electrolyte, while the CBs can serve as an active site for recapture or renucleation of small Pt clusters. These studies confirm the role of the RGO/CB hybrid structure in enhancing the catalyst durability. We have further demonstrated that the proposed working mechanism of the hybrid catalytic structure can be successfully applied to the commercial JM Pt/C product, which shows again greatly enhanced durability. This particular catalyst design approach can be used to prepare high-performance, durable fuel cell catalysts.

■ ASSOCIATED CONTENT

Ⓢ Supporting Information

TEM images and ADT results. This material is available free of charge via the Internet at http://pubs.acs.org.

■ AUTHOR INFORMATION

Corresponding Author

yhuang@seas.ucla.edu

Present Address

[§]China University of Petroleum, Beijing

Notes

The authors declare no competing financial interest.

■ ACKNOWLEDGMENTS

We acknowledge Electron Imaging Center of Nanomachines (UCLA) for the TEM facility and MIC in Department of Chemistry (UCLA) for the ICP-OES facility. Y.H. acknowledges support from ARO proposal no. 54709-MS-PCS and NSF grant no. CBET-1033672.

■ REFERENCES

(1) Gasteiger, H. A.; Markovic, N. M. *Science* **2009**, *324*, 48.
(2) Peng, Z.; Yang, H. *Nano Today* **2009**, *4*, 143.
(3) Li, Y.; Whyburn, G. P.; Huang, Y. *J. Am. Chem. Soc.* **2009**, *131*, 15998.
(4) Chiu, C.-Y.; Li, Y.; Ruan, L.; Ye, X.; Murray, C. B.; Huang, Y. *Nat. Chem.* **2011**, *3*, 393.
(5) Ruan, L.; Chiu, C.-Y.; Li, Y.; Huang, Y. *Nano Lett.* **2011**, *11*, 3040.
(6) Shao, Y.; Liu, J.; Wang, Y.; Lin, Y. *J. Mater. Chem.* **2009**, *19*, 46.
(7) Juntgen, H. *Fuel* **1986**, *65*, 1436.
(8) Huang, X.; Zhao, Z.; Fan, J.; Tan, Y.; Zheng, N. *J. Am. Chem. Soc.* **2011**, *133*, 4718.
(9) Koh, S.; Strasser, P. *J. Am. Chem. Soc.* **2007**, *129*, 12624.
(10) Habas, S. E.; Lee, H.; Radmilovic, V.; Somorjai, G. A.; Yang, P. *Nat. Mater.* **2007**, *6*, 692.
(11) Peng, Z.; Yang, H. *J. Am. Chem. Soc.* **2009**, *131*, 7542.
(12) Zhang, J.; Yang, H.; Fang, J.; Zou, S. *Nano Lett.* **2010**, *10*, 638.
(13) Wu, J.; Zhang, J.; Peng, Z.; Yang, S.; Wagner, F. T.; Yang, H. *J. Am. Chem. Soc.* **2010**, *132*, 4984.
(14) Li, W. Z.; Liang, C. H.; Zhou, W. J.; Qiu, J. S.; Zhou, Z. H.; Sun, G. Q.; Xin, Q. *J. Phys. Chem. B* **2003**, *107*, 6292.
(15) Zhou, Y.; Pasquarelli, R.; Holme, T.; Berry, J.; Ginley, D.; O'Hayre, R. *J. Mater. Chem.* **2009**, *19*, 7830.
(16) Shao, Y.; Sui, J.; Yin, G.; Gao, Y. *Appl. Catal., B* **2008**, *79*, 89.
(17) Geim, A. K.; Novoselov, K. S. *Nat. Mater.* **2007**, *6*, 183.
(18) Kou, R.; Shao, Y.; Mei, D.; Nie, Z.; Wang, D.; Wang, C.; Viswanathan, V. V.; Park, S.; Aksay, I. A.; Lin, Y.; Wang, Y.; Liu, J. *J. Am. Chem. Soc.* **2011**, *133*, 2541.
(19) Guo, S.; Sun, S. *J. Am. Chem. Soc.* **2012**, *134*, 4.
(20) Guo, S.; Dong, S.; Wang, E. *Acs Nano* **2010**, *4*, 547.
(21) Yoo, E.; Okata, T.; Akita, T.; Kohyama, M.; Nakamura, J.; Honma, I. *Nano Lett.* **2009**, *9*, 2255.
(22) Si, Y.; Samulski, E. T. *Chem. Mater.* **2008**, *20*, 6792.
(23) Seo, M. H.; Choi, S. M.; Kim, H. J.; Kim, W. B. *Electrochem. Commun.* **2011**, *13*, 182.
(24) Rao, C. V.; Reddy, A. L. M.; Ishikawa, Y.; Ajayan, P. M. *Carbon* **2011**, *49*, 931.
(25) Kou, R.; Shao, Y.; Wang, D.; Engelhard, M. H.; Kwak, J. H.; Wang, J.; Viswanathan, V. V.; Wang, C.; Lin, Y.; Wang, Y.; Aksay, I. A.; Liu, J. *Electrochem. Commun.* **2009**, *11*, 954.
(26) Liang, Y.; Li, Y.; Wang, H.; Zhou, J.; Wang, J.; Regier, T.; Dai, H. *Nat. Mater.* **2011**, *10*, 780.
(27) Choi, S. M.; Seo, M. H.; Kim, H. J.; Kim, W. B. *Carbon* **2011**, *49*, 904.
(28) Xin, Y.; Liu, J.-g.; Zhou, Y.; Liu, W.; Gao, J.; Xie, Y.; Yin, Y.; Zou, Z. *J. Power Sources* **2011**, *196*, 1012.
(29) Yoo, E.; Okada, T.; Akita, T.; Kohyama, M.; Honma, I.; Nakamura, J. *J. Power Sources* **2011**, *196*, 110.
(30) Gomez-Navarro, C.; Weitz, R. T.; Bittner, A. M.; Scolari, M.; Mews, A.; Burghard, M.; Kern, K. *Nano Lett.* **2007**, *7*, 3499.
(31) Yoo, E.; Kim, J.; Hosono, E.; Zhou, H.-s.; Kudo, T.; Honma, I. *Nano Lett.* **2008**, *8*, 2277.
(32) Park, S.; Shao, Y.; Wan, H.; Rieke, P. C.; Viswanathan, V. V.; Towne, S. A.; Saraf, L. V.; Liu, J.; Lin, Y.; Wang, Y. *Electrochem. Commun.* **2011**, *13*, 258.
(33) Hummers, W. S.; Offeman, R. E. *J. Am. Chem. Soc.* **1958**, *80*, 1339.
(34) Stankovich, S.; Dikin, D. A.; Piner, R. D.; Kohlhaas, K. A.; Kleinhammes, A.; Jia, Y.; Wu, Y.; Nguyen, S. T.; Ruoff, R. S. *Carbon* **2007**, *45*, 1558.
(35) Arenz, M.; Mayrhofer, K. J. J.; Stamenkovic, V.; Blizanac, B. B.; Tomoyuki, T.; Ross, P. N.; Markovic, N. M. *J. Am. Chem. Soc.* **2005**, *127*, 6819.
(36) Yan, J.; Wei, T.; Shao, B.; Ma, F.; Fan, Z.; Zhang, M.; Zheng, C.; Shang, Y.; Qian, W.; Wei, F. *Carbon* **2010**, *48*, 1731.
(37) Zhang, J.; Sasaki, K.; Sutter, E.; Adzic, R. R. *Science* **2007**, *315*, 220.
(38) Lim, B.; Jiang, M.; Camargo, P. H. C.; Cho, E. C.; Tao, J.; Lu, X.; Zhu, Y.; Xia, Y. *Science* **2009**, *324*, 1302.
(39) Ehrburger, P.; Mahajan, O. P.; Walker, P. L. *J. Catal.* **1976**, *43*, 61.
(40) Flynn, P. C.; Wanke, S. E. *J. Catal.* **1974**, *34*, 390.